Solubility Limit of Sol–Gel Grown Nano $Zn_{1-x}Mg_xO$ Through Charge Density Distribution

Santhanam Francis[a], Ramachandran Saravanan[a], and Mohammed Açıkgöz[b]

[a] Department of Physics, The Madura College, Madurai 625 011, India
[b] Bahcesehir University, Faculty of Arts and Sciences, Besiktas - 34349, Istanbul, Turkey

Reprint requests to R. S.; E-mail: saragow@dataone.in

Z. Naturforsch. **68a,** 668 – 676 (2013) / DOI: 10.5560/ZNA.2013-0043
Received March 14, 2013 / revised June 13, 2013 / published online July 31, 2013

The mixed oxides $Zn_{1-x}Mg_xO$ were prepared as polycrystalline powders with various compositions ($x = 0.02$, 0.04, 0.05, and 0.10) using sol–gel technique. X-ray diffractometer (XRD) was used to characterize the powders for structural and electronic properties. X-ray diffraction analysis reveals that all the prepared samples exhibit the single wurtzite phase of zinc oxide (ZnO), and magnesium-doping does not induce any secondary phase in the samples. The Bragg peak positions in the XRD patterns are found to be shifted towards higher 2θ values with more addition of magnesium in the zinc oxide lattice. Magnesium addition in the zinc oxide lattice is found to enhance the mid bond electron density distribution up to $x = 0.05$ and then decrease for $x = 0.10$. Evidence of host lattice as well as interstitial addition of Mg^{2+} ions has been realized for $x = 0.10$, through electron density analysis.

Key words: Oxides; X-Ray Diffraction; Sol–Gel; Structural Properties; Electronic Properties.

1. Introduction

Recently, various nanostructures of zinc oxide (ZnO) have attracted global interest and led to active research activities with possible applications in electronic, optoelectronic, and energy-conversion devices [1]. ZnO is an excellent electronic and photonic material having a wide band gap ($E_g \approx 3.27$ eV) and a large exciton binding energy of 60 meV. It crystallizes in a hexagonal wurtzite structure with lattice parameters of $a = 3.249$ Å, $c = 5.205$ Å. The ionic radius of Zn^{2+} is 0.60 Å [2]. ZnO is attracting considerable attention as one of the important candidates for potential applications including gas sensors, photodetectors, light-emitting diodes, varistors, piezoelectricity [3]. Therefore, many research groups concentrate on the subject of preparation and characterization of ZnO nanostructure.

In wide band gap semiconductors, the addition of impurities often induces dramatic changes in their electrical and optical properties [4], and some dopants such as magnesium, indium, aluminium, gallium, and cobalt have been successfully added to ZnO. Doping with magnesium may modulate the value of the band gap and increase the ultraviolet (UV) luminescence intensity [5]. $Zn_{1-x}Mg_xO$ is a semiconductor composed of two materials, zinc oxide and magnesium oxide (MgO), the growth of which can be easily controlled over a wide range of temperatures because the ionic radii of Mg^{2+} and Zn^{2+} are similar (0.57 Å and 0.60 Å, respectively) [6, 7]. Improvements in the growth of $Zn_{1-x}Mg_xO$ have led to many new applications in electronics and optoelectronics [8 – 10].

MgO (with a wide band gap of 7.7 eV) [3] doped ZnO material has attracted much attention because of its wider band gap compared to pure ZnO. $Zn_{1-x}Mg_xO$ has emerged as one of the promising compound semiconductors which is formed when magnesium is alloyed with ZnO. ZnO, which belongs to the wurtzite family, is a well known piezoelectric material, and alloying with MgO, which is non-piezoelectric and has the cubic rock salt structure, is reported to yield beneficial properties for piezoelectric device applications [11]. The composition of magnesium in the $Zn_{1-x}Mg_xO$ alloy determines the crystallographic structure, which can be tailored from the wurtzite phase of ZnO to the cubic phase of MgO [11].

According to Ghosh and Basak [12], for $Zn_{1-x}Mg_xO$ ($x = 0.0 – 0.20$) the X-ray diffraction (XRD) peaks could be indexed to a hexagonal wurtzite

ZnO structure for all the films with no other phase indicating these to be polycrystalline and single phase in the entire composition range. These results imply that the alloy oxide films retain the ZnO hexagonal wurtzite crystal structure up to $x = 0.20$. According to Fang and Kang [13], the intensities of crystalline (200) and (220) peaks increased as the $Mg(NO_3)_2$ concentration increased for Mg-doped ZnO nanorods. However, higher doping concentrations led to the degradation of the crystallinity of the nanorods. The width of the peak of the (002) plane decreased when the concentration of $Mg(NO_3)_2{\cdot}6H_2O$ was increased.

Wang et al. [14] found that with the increase in the dopant concentration, the peak position of (002) was shifted towards the high-angle side (from 34.40° to 34.50°). Further, Wang et al. [15] reported that magnesium ions introduced as dopants at levels below 10% shift the diffraction peaks to higher angles, suggesting that the unit cell contracts to accommodate the ions. Such a change is indeed to be expected if magnesium ions (0.57 Å) replace zinc ions (0.60 Å) in the lattice, as the magnesium ion has a smaller ionic radius. Higher levels of magnesium lead to a broadening of the peaks with shifts indicating as expansion of the unit cell, possibly due to the magnesium ions preferring to occupy interstitial sites.

However, only a limited number of reports are available on the structural studies of $Zn_{1-x}Mg_xO$ material at higher concentrations. Also, the electron density studies on Mg-doped ZnO have not been found. Hence, we have analysed the structural properties, phase, and electron densities of Mg-doped ZnO powder samples, and ascertained the doping level of magnesium ions that could be achieved through growth using the sol–gel method. In this paper, we report the growth of high-quality Mg-doped ZnO powders using the sol–gel technique with magnesium contents of $x = 0.02$, 0.04, 0.05, and 0.10. Then we carried out a detailed study on the structural and electronic properties of $Zn_{1-x}Mg_xO$ powder samples. The effect of Mg-doping on the electronic structure of doped ZnO bulk samples is analyzed in detail.

2. Experimental

The mixed oxides $Zn_{1-x}Mg_xO$ were prepared as polycrystalline powders with various compositions ($x = 0.02$, 0.04, 0.05, and 0.10) using the sol–gel technique. Zinc acetate dihydrate (Fluka) and magnesium 2,-4-pentanedionate (Alfa Easer) were used as precursor materials. Methanol and acetyl acetone were used as solvents and chelating agent. After weighing the appropriate amount of the constituents, they were put all together in a Pyrex container and mixed with a magnetic stirrer for about 8 hours at room temperature until a transparent solution was obtained. The precursor solution was stable at room temperature. After solutions become transparent, container cover was opened and they were rotated to remove the solvent at room temperature using a magnetic stirrer. Then the powders were ground, annealed at 600 °C for 30 min under air in a box furnace.

The synthesized samples were characterized by powder X-ray (CuK_α) diffraction (Philips, X- PERT PRO, Netherland) at room temperature. The wavelength used for X-ray intensity data collection was 1.54056 Å. The 2θ range of data collection was 20° to 90° for all the data sets with the step size 0.05 in 2θ.

3. Result and Discussion

3.1. XRD and Rietveld Refinement Analysis

The X-ray diffraction analysis was used to find phase and crystal structure of the Mg-doped ZnO powder samples. Figure 1 represents Bragg peaks of (100) Bragg reflection, respectively, for $x = 0.02$, 0.04, 0.05, and 0.10. It is observed that the intensities of the Bragg reflections are found to be increased with an increase in the doping concentrations. It clearly indicates that the

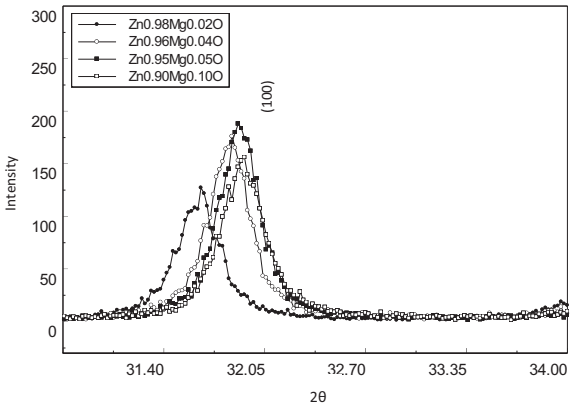

Fig. 1. XRD peaks of (100) Bragg reflection of the $Zn_{1-x}Mg_xO$ powder samples for $x = 0.02$, 0.04, 0.05, and 0.10.

crystallinity gets improved with the increase in doping concentration. The XRD patterns on the four samples show that there are shifts in the Bragg positions of all the observed Bragg peaks up to $x = 0.10$, towards higher 2θ values. The peak positions are shifted toward the high-side angle with respect to the doping level, indicating that Mg^{2+} has incorporated into the ZnO host lattice and substitutes for Zn^{2+}, as the ionic radius of Mg^{2+} (0.57 Å) is smaller than Zn^{2+} (0.60 Å) [16]. It is also found that, the shifts of peaks from $Zn_{0.98}Mg_{0.02}O$ to $Zn_{0.96}Mg_{0.04}O$ is large, but the shift of peaks from $Zn_{0.95}Mg_{0.05}O$ to $Zn_{0.90}Mg_{0.10}O$ is much smaller. This may be due to the saturation of magnesium doping in ZnO, and some MgO may exist as impurities at $x = 0.10$.

The crystalline size of Mg-doped ZnO is calculated by substituting values of full width at half maximum (FWHM) in the Scherrer formula [17],

$$D = \frac{K\lambda}{\beta \cos\theta}, \tag{1}$$

where D is the crystalline size of the crystal, the constant K is the shape factor $= 0.9444$, λ is the wavelength of X-rays (1.5406 Å for CuK_α), θ is the Bragg angle, and β is the FWHM. The crystalline size of the grown nano $Zn_{1-x}Mg_xO$ samples are shown in Table 1. The crystallite size measured by using the Scherrer equation was found to increase up to $x = 0.05$ and then decreases for $x = 0.10$. The crystalline nature of powders was affected due to the enhancement of dopant concentration, by which more impurities were included in the ZnO crystal.

The cell parameters were refined using the unit cell [18] software for all the powder samples. In the Rietveld refinement analysis of the structure, all the essential structural and profile parameters are refined using the software package Jana 2006 [19] to get accurate information on the structure. Figure 2a – d show the XRD pattern of the Rietveld refined profile for four samples. As seen from these figures, all the sharp diffraction peaks in the pattern can be easily assigned to hexagonal phase ZnO (wurtzite-type, space group: $P6_3mc$). No other phases have been found, revealing that magnesium doping has not changed the wurtzite structure of ZnO because of its small content. In addition, the sharp diffraction peaks reveal that the prepared samples possess good crystalline quality. The wurtzite structure lattice parameters are shown in Table 2. In general, the lattice constants a and c of Mg-doped powders are smaller than those of pure ZnO ($a = 3.250$ Å, $c = 5.205$ Å at room temperature).

Table 1. X-ray derived particle size of $Zn_{1-x}Mg_xO$.

Dopant Concentration (x)	Crystalline size (nm)
0.02	45.99
0.04	46.93
0.05	48.30
0.10	46.94

Labuayai et al. [3] have reported on XRD patterns showing exactly the same peak patterns, which can be indexed as the ZnO wurtzite structure data (JCPDS, 36-1451). However, the presence of a second phase as MgO (JCPDS, 45-0946) was observed with a magnesium concentration of $x \geq 0.2$, and also a reduction in the cell parameters a and c of Mg-doped ZnO up to $x = 0.40$. Chakrabarti et al. [20] have also reported on XRD peaks that could be indexed to a hexagonal wurtzite ZnO structure and decreased in both a and c cell parameters of Mg-doped ZnO for x values from 0 to 0.15. A shift in the XRD peaks of Mg-doped ZnO is found by Zhuang et al. [16] and Haiping Tang et al. [1]. C axis contraction of Mg-doped ZnO has been presented by Kumar et al. [11], Wang et al. [15], and Wang et al. [14]. Also, no structural change was reported by

Table 2. Structural parameters of $Zn_{1-x}Mg_xO$ from Rietveld refinement.

Parameter	Refinement values			
	$x = 0.02$	$x = 0.04$	$x = 0.05$	$x = 0.10$
a (Å)	3.2445(2)	3.2437(4)	3.2426(3)	3.2394(8)
c (Å)	5.1952(2)	5.1927(3)	5.1883(5)	5.1866(7)
z (O)	0.8750(1)	0.8651(3)	0.8749(5)	0.8749(2)
R_{obs} (%)	0.85	1.21	0.91	0.96
wR_{obs} (%)	0.78	1.11	1.21	0.96
R_p (%)	4.22	5.95	5.34	5.60
wR_p (%)	7.51	11.28	9.34	10.03

z - fractional atomic coordinate of oxygen atom

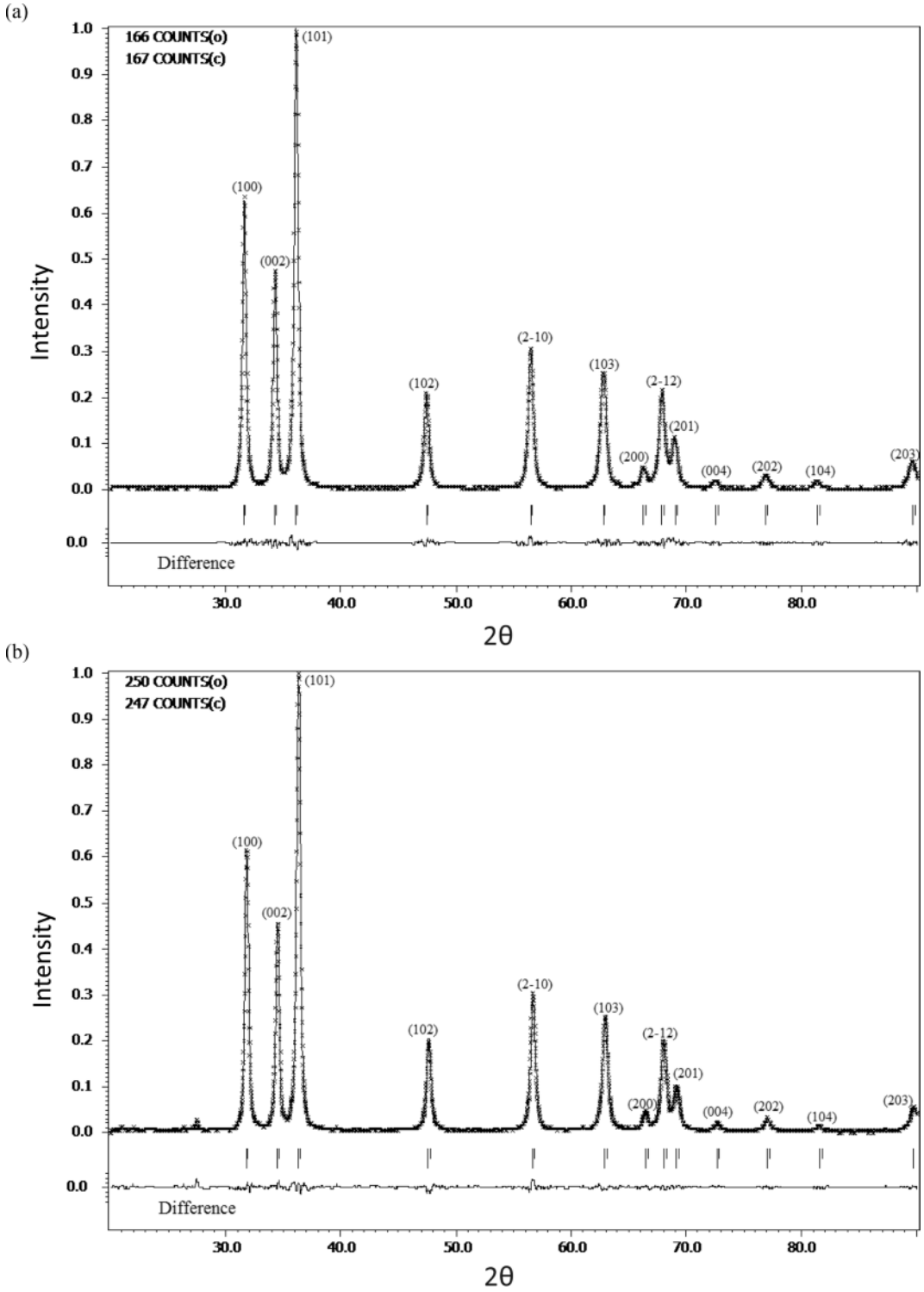

Fig. 2. Rietveld refined profiles for $Zn_{1-x}Mg_xO$ (a) $x = 0.02$, (b) $x = 0.04$.

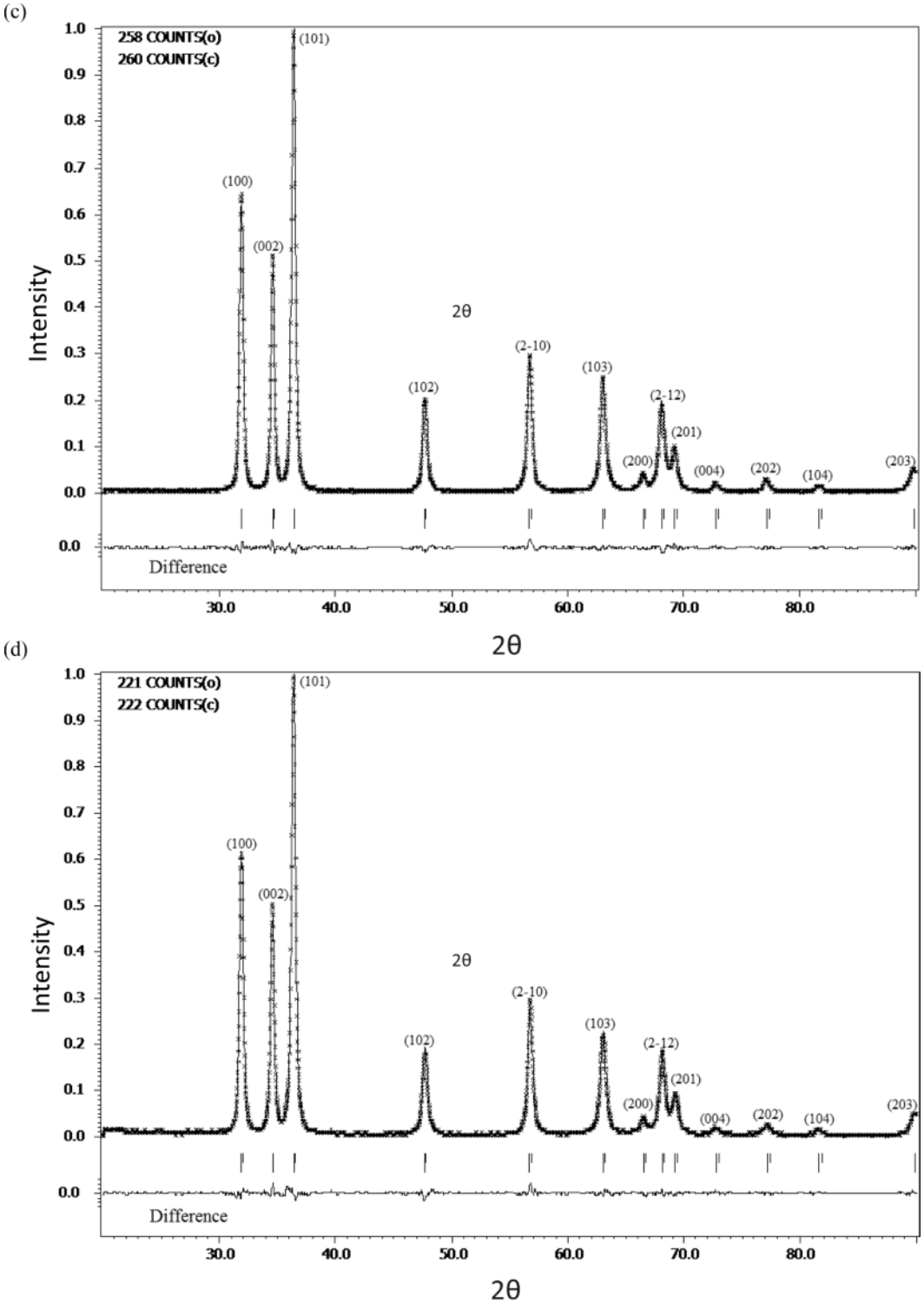

Fig. 2. (continued). Rietveld refined profiles for $Zn_{1-x}Mg_xO$ (c) $x = 0.05$, (d) $x = 0.10$.

Table 3. Parameters from the MEM analysis of $Zn_{1-x}Mg_xO$.

Parameter	$x = 0.02$	$x = 0.04$	$x = 0.05$	$x = 0.10$
Number of cycles	4180	3697	3687	4326
Lagrange parameter (λ)	0.00052	0.00047	0.00046	0.00053
R_{MEM} (%)	0.0232	0.0200	0.0207	0.0223
wR_{MEM} (%)	0.0225	0.0196	0.0205	0.0215

Li et al. [5] up to an x value of $x = 0.15$ in Mg-doped $Zn_{1-x}Mg_xO$.

Our XRD results also show a shrinkage in the lattice parameters up to $x = 0.10$ and indicate the proper incorporation of magnesium in to the ZnO lattice. But for $x = 0.10$, there might be an addition of magnesium in the interstitial sites too as evidenced by our electron density studies. Figure 1 shows that while there is a shift in the XRD peaks towards higher angle sides, for $x = 0.10$ the intensity was reduced compared to the other compositions $x = 0.04$ and $x = 0.05$, and was comparable to the intensity corresponding to $x = 0.05$. This indicates that for $x = 0.10$, while there is an incorporation of Mg^{2+} in the host lattice ZnO, there may also occur an interstitial substitution of Mg^{2+} which leads to a comparable reduction in intensity for $x = 0.10$ as evidenced from our electron density studies.

3.2. MEM Analysis

The maximum entropy method (MEM) is a method to derive the most probably map given by a set of experimental data. In crystallography, MEM can be used to determine the electron density in the unit cell that provides the best fit to the scattering data. This method is acknowledged as the super resolution technique which can reveal the most intricate information of the systems concerned. Studies using MEM in understanding different types of bonding and the interior electronic details of many materials

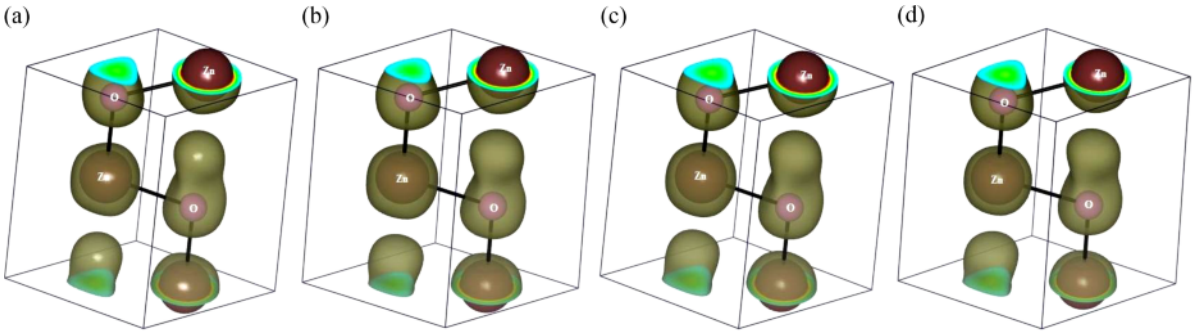

Fig. 3 (colour online). Three-dimensional charge density of $Zn_{1-x}Mg_xO$ in the unit cell (a) $x = 0.02$, (b) $x = 0.04$, (c) $x = 0.05$, (d) $x = 0.10$.

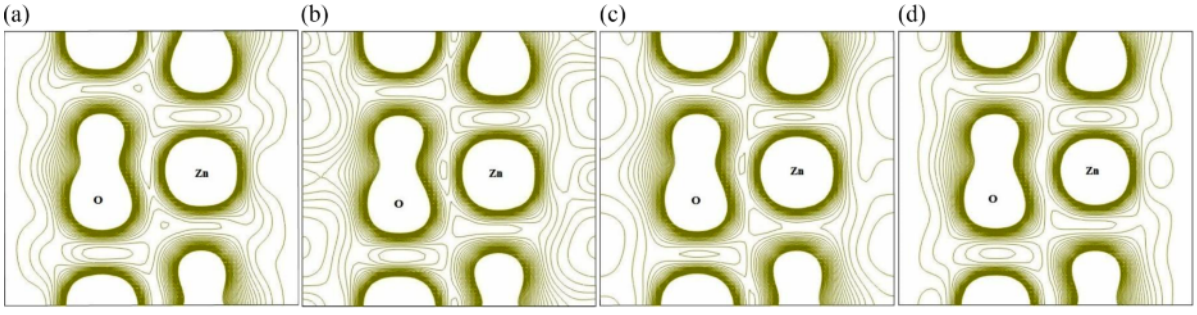

Fig. 4 (colour online). Two-dimensional MEM electron density distribution of $Zn_{1-x}Mg_xO$ on the (110) plane. (a) $x = 0.02$, (b) $x = 0.04$, (c) $x = 0.05$, (d) $x = 0.10$. (Contour range is from 0.02 to 1.5 $e/Å^3$, contour interval is 0.05 $e/Å^3$, and distance from the origin is 1.6 Å).

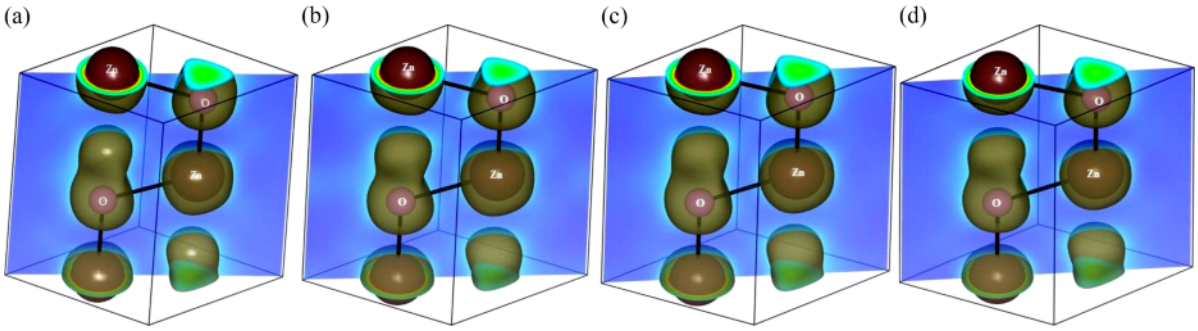

Fig. 5 (colour online). Three-dimensional isosurface of $Zn_{1-x}Mg_xO$ showing the (110) plane. (a) $x = 0.02$, (b) $x = 0.04$, (c) $x = 0.05$, (d) $x = 0.10$.

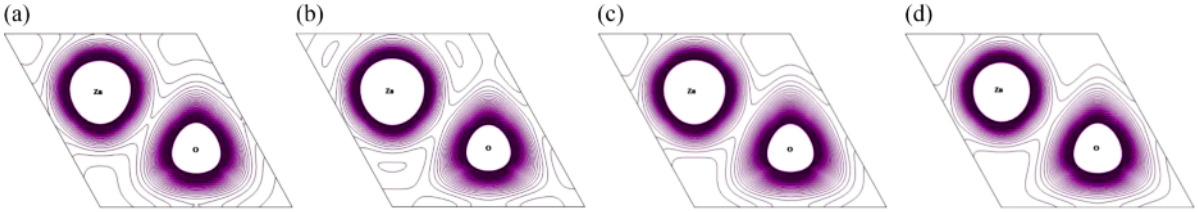

Fig. 6 (colour online). Two-dimensional MEM electron density distribution of $Zn_{1-x}Mg_xO$ on the (002) plane. (a) $x = 0.02$, (b) $x = 0.04$, (c) $x = 0.05$, (d) $x = 0.10$. (Contour range is from 0.02 to 3 $e/Å^3$, contour interval is 0.05 $e/Å^3$, and distance from the origin is 2.2 Å).

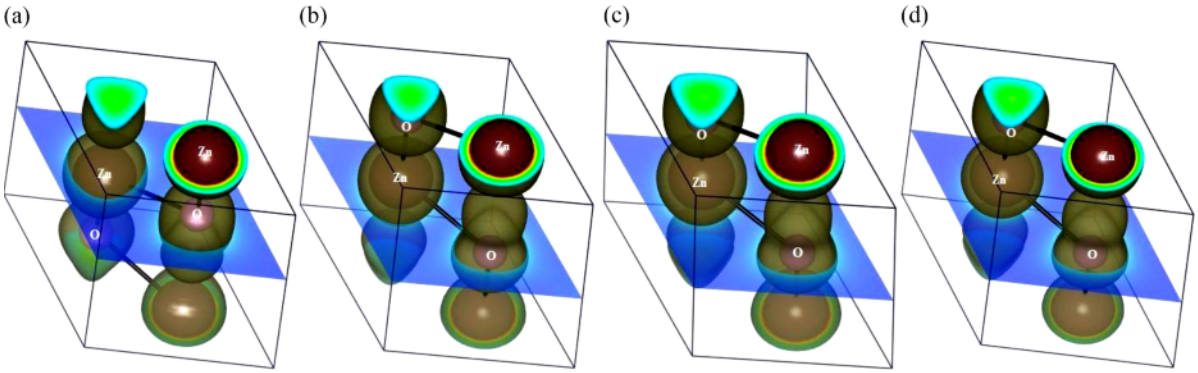

Fig. 7 (colour online). Three-dimensional isosurface of $Zn_{1-x}Mg_xO$ showing the (002) plane. (a) $x = 0.02$, (b) $x = 0.04$, (c) $x = 0.05$, (d) $x = 0.10$.

are available in literature (e. g., Yamamura et al. [21], Gilmore [22]). The method adopted for the charge density reconstruction is a versatile tool used in information technology [23].

The electronic structure of $Zn_{1-x}Mg_xO$ in one, two, and three dimensions with $x = 0.02$, 0.04, 0.05, and 0.10 is analyzed by MEM [24] using the structure factors obtained from X-ray measurements. The MEM electron densities compiled from the experimental information are applied for the visualization of the three-dimensional electron density using the software VESTA [25]. The space groups of these systems were taken as $P6_3mc$. The MEM electron density studies have been carried out as mentioned in research papers published by one of the authors [26 – 28]. The three-dimensional charge density distribution of wurtzite $Zn_{1-x}Mg_xO$ in the unit cell is shown in Figure 3a – d for $x = 0.02$, 0.04, 0.05, and 0.10, respectively. In general, the size of the isosurface corresponding to the zinc atom is reduced with doping element

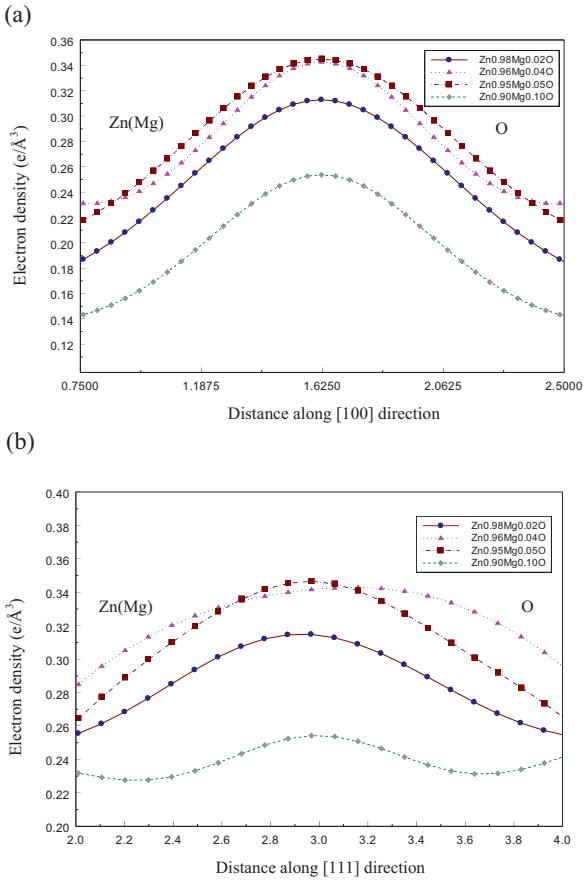

Fig. 8. (a) One-dimensional variation of electron density between Zn and O along [100] direction, for $x = 0.02$, $x = 0.04$, 0.05, and $x = 0.10$.
(b) One-dimensional variation of electron density between Zn and O along [111] direction, for $x = 0.02$, $x = 0.04$, 0.05, and $x = 0.10$.

magnesium. The decrease in the isosurface is due to the smaller ionic radius of the Mg^{2+} ion (0.57 Å) substituting the larger host ion Zn^{2+} (0.60 Å) at its site in ZnO. The parameters of MEM analysis are presented in Table 3.

Figure 4a–d shows the two-dimensional electron densities of $Zn_{1-x}Mg_xO$ on the (110) plane for $x =$ 0.02, 0.04, 0.05, and 0.10, respectively. The (110) plane along with the three-dimensional isosurfaces of the electron clouds in the unit cell is presented in Figure 5a–d for $x = 0.02$, 0.04, 0.05, and 0.10. We have analysed the electron densities on the (002) plane too, which is located at a distance of 2.2 Å from the origin. Figure 6a–d show the two-dimensional representations of the electron densities on the (002) plane. The three-dimensional isosurfaces and the (002) plane are shown in Figure 7a–d for $x = 0.02$, 0.04, 0.05, and 0.10. These figures clearly reveal the reduction of the charge distribution of the host zinc atom when the concentration of magnesium is increased.

The host lattice addition of Mg^{2+} for Zn^{2+} leads to a shrinkage of the lattice and hence more close interaction of zinc (magnesium) and oxygen atoms which leads to slightly increased bond charges as seen from Table 4. For $x = 0.10$, there may be an interstitial addition of Mg^{2+} ions in addition to the host lattice addition of Mg^{2+} which might cause a complicated lattice and hence a slight reduction in the mid bond electron density along the [100] and [111] direction in the unit cell. The electron density maps clearly reveal the reduction of the charge distribution of the host atom zinc when the concentration of magnesium is increased.

The one-dimensional electron density profiles are shown in Figure 8a and b for the bonding between zinc and oxygen atom along the [100] and [111] direction, respectively. The values of the mid bond densities are given in Table 4. In both cases, it shows increasing electron densities with respect to increasing magnesium content up to $x = 0.05$, it then decreases for $x = 0.10$. This is due to a closer interaction of zinc (magnesium) and oxygen atoms up to $x = 0.05$, which is only possible through more host lattice addition of Mg^{2+}. While the two- and three-dimensional analyses show an inclusion of Mg^{2+} in the zinc host lattice, the mid bond densities through the one-dimensional analyses also show that there is a host lattice addition of magnesium in the form of Mg^{2+} up to $x = 0.05$. This implies that the solubility limit for magnesium doping in $Zn_{1-x}Mg_xO$ sample using sol–gel method is up to $x = 0.05$. Ghosh and Basak [12] reported that when magnesium is substituted in ZnO using the sol–

Table 4. Electron densities of $Zn_{1-x}Mg_xO$ in the Zn(Mg)-O bond.

x	Direction	
	[100] Electron density (e/Å^3)	[111] Electron density (e/Å^3)
0.02	0.312	0.315
0.04	0.342	0.345
0.05	0.345	0.346
0.10	0.254	0.254

gel method, an equilibrium solid solution is formed up to $x = 0.05$ in accordance with the thermodynamical solubility limit. Chakrabarti et al. [20] observed that the band gap of the sol–gel grown $Mg_xZn_{1-x}O$ films was increased with increasing the magnesium concentration. The annealing of the films in static oxygen atmosphere substantially reduces the defect related emission and increases the near band edge UV emission of the films. For the UV emission intensity to be maximum, the optimum x value is $x = 0.05$. The parameters involved in electron densities of $Zn_{1-x}Mg_xO$ in the $Zn(Mg) - O$ bond analysis are presented in Table 4.

4. Conclusion

The mixed oxides $Zn_{1-x}Mg_xO$ were prepared with various compositions using sol–gel technique at 600 °C for 30 min. The present results revealed that the Mg-doping has not changed the wurtzite phase of ZnO, indicating that phase-pure doping was obtained. The mid bond electron densities are increasing with magnesium contents up to $x = 0.05$, then decreases for $x = 0.10$, leading to the conclusion that the solubility limit for Mg-doping using sol–gel method is around 5%.

[1] H. Tang, B. J. Kwon, and Ji-Y. Park, Phys. Stat. Sol. **207**, 2478 (2010).
[2] N. Kılınç, L. Arda, S. Öztürk, and Z. Z. Öztürk, Cryst. Res. Technol. **45**, 529 (2010).
[3] S. Labuayai, V. Promarak, and S. Maensiri, Optoelect. Adv. Mat. **2**, 798 (2008).
[4] F. K. Shan, K. I. Kim, G. X. Liu, Z. F. Liu, and J. Y. Sohn, J. Appl. Phys. **95**, 4772 (2004).
[5] J. Li, H. Zhuang, J. Wang, and P. Xu, Phys. Stat. Sol. **208**, 136 (2011).
[6] A. Umar, S. H. Kim, J. H. Kim, A. Al-Hajry, and Y. B. Hahn, J. Alloys Compd. **463**, 516 (2008).
[7] D. K. Hwang, M. C. Jeong, and J. M. Myoung, Appl. Surf. Sci. **225**, 217 (2004).
[8] T. H. Fang and S. H. Kang, J. Appl. Phys. **105**, 113512 (2009).
[9] H. Yang, Y. Li, D. P. Norton, S. J. Pearton, S. Jung, F. Ren, and L. A. Boatner, Appl. Phys. Lett. **86**, 172103 (2005).
[10] S. Sasa, M. Ozaki, K. Koike, M. Yano, and M. Inoue, Appl. Phys. Lett. **89**, 53502 (2006).
[11] S. Kumar, V. Gupte, and K. Sreenivas, J. Phys.: Condens. Matter **18**, 3343 (2006).
[12] R. Ghosh and D. Basak, J. Appl. Phys. **101**, 23507 (2007).
[13] Te-H. Fang and S.-H. Kang, J. Alloys Compd. **492**, 536 (2010).
[14] F. Wang, C. Zhao, B. Liu, and S. Yuan, J. Phys. D: Appl. Phys. **42**, 115411 (2009).
[15] Y. S. Wang, P. J. Thomas, and P. O'Brien, J. Phys. Chem. B **110**, 21412 (2006).
[16] H. Zhuang, J. Wang, H. Liu, and P. Xu, Acta Phys. Polon. A **119**, 819 (2011).
[17] N. Murugesan and A. Achuthanunni, J. Sci. Technol. **18**, 81 (2010).
[18] T. J. B. Holland and S. A. T. Redfern, Mineral. Mag. **61**, 65 (1997).
[19] V. Petříček, M. Dušek, and L. Palatinus, JANA 2006, The Crystallographic Computing System, Institute of Physics, Academy of sciences of the Czech republic, Praha 2006.
[20] S. Chakrabarti, S. Kar, A. Dev, and S. Chaudhuri, Phys. Stat. Sol. A **202**, 441 (2005).
[21] S. Yamamura, M. Takata, M. Sakata, and Y. Sugawara, J. Phys. Soc. Jpn. **67**, 4124 (1968).
[22] C. J. Gilmore, Acta Cryst. A **52**, 561 (1996).
[23] D. M. Collins, Nature **49**, 298 (1982).
[24] F. Izumi and R. A. Dilanian, Recent Research Developments in Physics, Vol. 3, Part II, Transworld Research Network, Trivandrum 2002, 699–726.
[25] K. Momma and F. Izumi, J. Appl. Crystallogr. **41**, 653 (2008).
[26] R. Saravanan and M. P. Rani, J. Phys.: Cond. Mat. **19**, 1 (2007).
[27] R. Saravanan, K. S. S. Ali, and S. Israel, Pramana **70**, 679 (2008).
[28] R. Saravanan, S. Francis, and L. J. Berchmans, Chem. Papers **66**, 226 (2012).